

# Deciphering the Thermodynamic Landscape of CRISPR/Cas9: Insights into Enhancing Gene Editing Precision and Efficiency

Ajit Kumar, Purba Daripa, Kaiser Rasool, Debojyoti Chakraborty, Niyati Jain,\* and Souvik Maiti\*



Cite This: *J. Phys. Chem. B* 2024, 128, 8409–8422



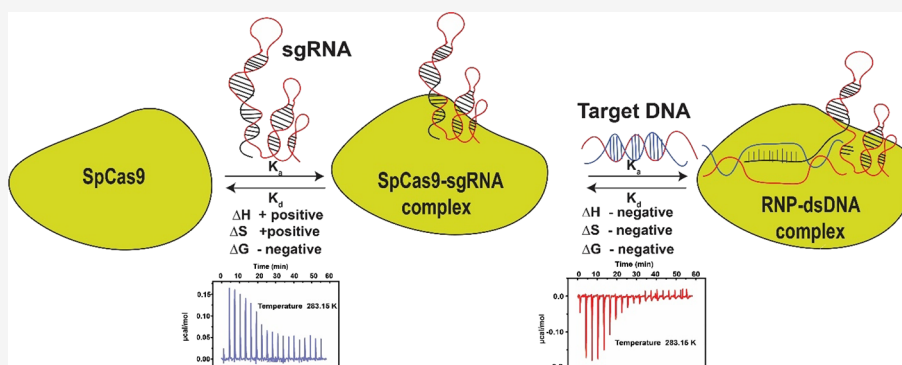
Read Online

ACCESS |

Metrics & More

Article Recommendations

Supporting Information



**ABSTRACT:** The thermodynamic landscape of the CRISPR/Cas9 system plays a crucial role in understanding and optimizing the performance of this revolutionary genome-editing technology. In this research, we utilized isothermal titration calorimetry and microscale thermophoresis techniques to thoroughly investigate the thermodynamic properties governing CRISPR/Cas9 interactions. Our findings revealed that the binding between sgRNA and Cas9 is primarily governed by entropy, which compensates for an unfavorable enthalpy change. Conversely, the interaction between the CRISPR RNP complex and the target DNA is characterized by a favorable enthalpy change, offsetting an unfavorable entropy change. Notably, both interactions displayed negative heat capacity changes, indicative of potential hydration, ionization, or structural rearrangements. However, we noted that the involvement of water molecules and counterions in the interactions is minimal, suggesting that structural rearrangements play a significant role in influencing the binding thermodynamics. These results offer a nuanced understanding of the energetic contributions and structural dynamics underlying CRISPR-mediated gene editing. Such insights are invaluable for optimizing the efficiency and specificity of CRISPR-based genome editing applications, ultimately advancing our ability to precisely manipulate genetic material in various organisms for research, therapeutic, and biotechnological purposes.

## INTRODUCTION

Clustered regularly interspaced short palindromic repeats (CRISPR) and their associated proteins, known as CRISPR-Cas systems, are revolutionary tools in the field of genetic engineering and molecular biology. These systems were originally discovered as part of the bacterial immune system, where they provide defense against viral infections. The CRISPR-Cas system has been adapted for use in various biotechnological applications, including gene editing. Recent developments in CRISPR/Cas9 gene editing technologies unlike their counterpart meganucleases, transcription activator-like effector nucleases, and zinc finger nucleases (ZFN) have been fruitful,<sup>1</sup> as CRISPR/Cas9 system can edit genomes more efficiently and with significant specificity.<sup>1</sup>

Today, gene editing using CRISPR-Cas9 technology has revolutionized biological research. This breakthrough is largely due to the efforts of researchers who have deeply explored and elucidated the functional mechanisms of the CRISPR-Cas system.<sup>2–4</sup> This sought Cong et. al to harness *Streptococcus*

*pyogenes* RNA-guided Cas9 nuclease activity in editing eukaryotic cells.<sup>5</sup> The *S. pyogenes* Cas9 protein, which is commonly used for genome editing in the CRISPR system, belongs to the type II CRISPR system. Furthermore, the crystal structure for this type II CRISPR system revealed the precise functional interactions between *S. pyogenes* Cas9 and sgRNA and its target DNA,<sup>6</sup> although crystal structure determined the spatial pattern of the SpCas9–sgRNA–DNA complex but failed to capture structural rearrangements that happen during the complex formation. Thus, additional structural studies harnessing single molecule spectroscopy,

Received: June 18, 2024

Revised: August 2, 2024

Accepted: August 19, 2024

Published: August 27, 2024



**Table 1.** Sequences of sgRNA and the VEGFA3 Target and Nontarget Strand of DNA

template	sequences
sgRNA	GGUGAGUGAGUGUGUGCGUGGUUUUAGAG-CUAGAAAUAUGCAAGUAAAUAAGGCUAGUCGUUAUCAACUUGAAAAAGUGGC
VEGFA3_target_F.P_Sp	TGTGGGTGAGTGAGTGTGCGTGTGGGGT
VEGFA3_target_R.P_Sp	ACCCACACGACACACTCACTACCCACA

nuclear magnetic resonance, high-speed atomic force microscopy, and molecular dynamic simulation provide insights into the dynamic behavior of the SpCas9 system and its interplay with RNA/DNA.<sup>7–10</sup>

Recently, more studies have focused on enhancing the CRISPR-Cas9 system's efficiency while minimizing off-target effects. One computational study identified amino acid targets that can destabilize mismatch-containing systems, a potential approach to reducing off-target effects.<sup>11</sup> Additionally, cryo-EM structures explored the metal coordination in the RuvC domain, to create a Cas9 variant with altered metal ion specificity. This modification could expand the applications of CRISPR-Cas9.<sup>12</sup> Another recent study focused on the kinetic mechanism of Cas9 that provided insights into specific catalytic steps that could be targeted to prevent off-target DNA cleavage during gene editing. Additionally, dsDNA cleavage is regulated by the kinetics of HNH and RuvC domain movements, and the studies further show how protein engineering can modulate Cas9's conformational dynamics to minimize off-target effects.<sup>13</sup> In recent years, extensive studies have been conducted to enhance the efficiency of the Cas9 system and reduce its off-target effects. However, there has been a lack of research focused on measuring the binding thermodynamics and exploring the energetic landscape of the SpCas9–sgRNA and SpCas9–sgRNA–DNA complexes. This understanding is essential, as the complex interplay between guide RNA, target DNA, and SpCas9 protein is fundamental to enhancing the functionality of CRISPR-Cas9 technology.

The binding energy between these components is vital for the stability of the complex and the efficiency of the CRISPR system. In a biological environment, various factors can influence these interactions, such as temperature, pH, and the presence of osmolytes and other biomolecules. Mimicking the conditions of the biological environment is crucial for studying and utilizing these molecular interactions effectively. Our study focuses on investigating the impact of various factors such as temperature, osmolytes, and ion presence on the binding interactions between SpCas9–sgRNA and RNP–dsDNA, aiming to closely simulate biological environments. These studies will likely provide insights into the energetic aspects, changes in hydration, and conformational states that drive these interactions. Our work carries significant implications, as a comprehensive understanding of the underlying thermodynamics through the combination of calorimetry and MST has the potential to enhance and broaden its applicability.

## MATERIAL AND METHODS

**Protein Purification.** The plasmid encoding full-length SpCas9 nuclease (WT) cloned in the pET-28b expression vector was purchased from Addgene (68705). Catalytically inactive SpCas9 double mutants (dSpCas9) were generated on the plasmid backbone by a Quick-change II site-directed mutagenesis kit (Agilent) following the standard protocol. Plasmid construct encoding SpCas9 (WT), dSpCas9, and 6x

His–MBP–dSpCas9gfp were transformed in Rosetta and BL21DE3. The bacterial cells were cultured at 37 °C in Luria–Bertani (LB) medium, supplemented with the antibiotics, until reaching an optical density at 600 nm (OD600) of 0.6. Subsequently, induction was initiated by adding 0.2 mM isopropyl β-d-thiogalactopyranoside (IPTG). Following induction, the cells were allowed to grow at 20 °C overnight and were harvested. The protein purification was done as discussed previously.<sup>14</sup> The eluted protein was further purified by gel-filtration chromatography in ITC buffer (20 mM Tris-HCl pH 7.5, 150 mM NaCl, 10 mM MgCl<sub>2</sub>, 2 mM TCEP). For the MST experiments, dSpCas9 was expressed and purified as a GFP fusion protein as reported previously.<sup>15</sup> The cleaved dSpCas9gfp protein was purified and separated from the fusion tag on the HiLoad Superdex 200 column (GE Healthcare) in a standard MST buffer.

**RNA/DNA Preparation.** A chemically synthesized DNA template encoding a single guide RNA (sgRNA) sequence in Table 1 along with the upstream T7 Promoter sequence was cloned into the Pcr2.1 TOPA plasmid vector. The linear DNA template for in vitro transcription (IVT) was PCR amplified using primer sequences in Table 1. RNA samples were prepared by in vitro transcription using T7 RNA polymerase. Transcription buffer (30 mM Tris pH 8, 2 mM spermidine, 25 mM MgCl<sub>2</sub>, 0.01% Triton-X100, DTT 2 mM, 5% DMSO), T7 RNA polymerase, DNA template, and rATP, rCTP, rGTP, and rUTP (biosynth UK) were incubated at 37 °C for 8–10 h. Following IVT, RNA constructs were purified using 8% denaturing PAGE. The RNA band was detected through UV shadowing, and subsequently, the identified band was carefully excised. Afterward, the RNA was eluted from the gel bands through the elutrap system using dialysis tubing (pore size 2000 NMWCO Sigma). The RNA was then exchanged into nuclease-free water (Himedia) and concentrated using the 10 kDa Millipore Amicon concentrator. The size and overall integrity of sgRNA were assessed by denaturing and native PAGE, respectively. The RNA was stored at –20 °C before use. An online calculator was used to determine the theoretical molar extinction coefficient to calculate the concentration of sgRNA.

**dsDNA Preparation.** The dsDNA VEGFA\_site 3 (VEGFA3) was used as the target substrate in this study to understand the binding interactions between SpCas9–sgRNA–dsDNA. The dsVEGFA3 DNA was previously used as a target substrate to comprehend the binding between the FnCas9–sgRNA–dsDNA.<sup>15</sup> The synthetic dsDNA VEGFA3 (30 nucleotides) encompassing the target DNA strand and nontarget DNA strand with 5'-TGG-3' PAM sequence HPLC purified was purchased from Bioserve A Reprocell Company, Hyderabad, Telangana India. Both strands were mixed at a 1:1 molar ratio, heated at 95 °C for 3–5 min, and then allowed to anneal at room temperature for 30 min to form a dsDNA duplex.

**Isothermal Titration Calorimetry.** Calorimetric titrations were conducted over a spectrum of temperatures (283.15–

309.15 K) employing a Microcal PEAQ-ITC instrument (Malvern Panalytical). The sgRNA was prepared for titration by heating at 95 °C for 3 min, succeeded by rapid cooling on ice, and then exchanged into the ITC buffer using the Amicon concentrators. Through a series of 19 injections (2  $\mu$ L each), sgRNA concentrations ranging from 20 to 50  $\mu$ M were titrated into 300  $\mu$ L of 2.5–5  $\mu$ M 6 × His-dSpCas9 protein.

The complex for sgRNA and dSpCas9 was prepared at a 1:3 ratio to ensure the absence of free sgRNA, as unbound sgRNA could potentially hybridize with complementary ssDNA, leading to the release of heat. The sgRNA to dSpCas9 RNP (1:3) was mixed and incubated at 21 °C for an hour for complex formation. Subsequently, 80–100  $\mu$ M preannealed dsDNA VEGFA3 targets were titrated on the 2–3  $\mu$ M RNP complex. All experiments were conducted in triplicate. The control experiments were carried out wherein sgRNA and dsDNA were titrated into the buffer independently, generating a negligible heat. The titration data were analyzed using the MicroCal PEAQ-ITC analysis software. The software employed the fitted offset option, automatically subtracting the control heat from the titration. The resulting isotherm was fitted using a one set of site binding model.

**Nano Differential Scanning Fluorimetry.** NanoDSF analysis was conducted employing a Prometheus NT.48 instrument (NanoTemper Technologies, Munich, Germany). The samples were filled in nanoDSF-grade standard capillaries (NanoTemper Technologies). The samples were subjected to a gradual temperature increase, starting from 20 to 80 °C at a ramp rate of 1 °C per minute. The samples of SpCas9 (WT) protein and SpCas9–sgRNA (1:1) RNP complex were prepared in the presence of an increasing concentration of osmolytes (glycerol and sucrose, 0–40%), and melting scans were collected after 10 min incubation. Following UV excitation at 280 nm, the fluorescence emission spectra of tryptophan were recorded using a dual-UV detector at both wavelengths 330 and 350 nm wavelengths. Since the ratio of the two wavelengths did not result in a meaningful first derivative curve, so the data collected at a single wavelength (330 nm) was further analyzed to get the thermal melting temperature. The changes in the fluorescence of tryptophan and the first derivative were calculated using the PR.Therm-Control software. Thermal stability parameters such as  $T_{\text{onset}}$  and  $T_m$  were subsequently calculated.

**UV Melting.** Thermal melting experiments were conducted on free SpCas9 and SpCas9–sgRNA complex (1:1) using an Agilent Cary 3500 UV-vis spectrophotometer. The experiments were performed at a 2  $\mu$ M concentration of free protein in ITC buffer, and similar concentrations of protein were used for complex formation (SpCas9–sgRNA) in the presence of varying salt concentrations (NaCl 150–600 mM). The samples were heated from 20 to 80 °C at a steady rate of 1 °C per minute, and absorbance was monitored at 280 nm at intervals of 0.1 °C. Each melting curve was subjected to duplicate measurements. The melting temperature ( $T_m$ ) was established utilizing OriginPro 8.5 for Windows, employing analysis of the first-order derivatives of absorbance against temperature.

**Microscale Thermophoresis.** MST binding experiments were performed using the Monolith NT.115 instrument (Nanotemper Technologies). Binding experiments were conducted across a temperature range of 295.15–309.15 K. Additionally, investigations were undertaken to assess the impact of increased osmolyte (glycerol and sucrose)

concentrations (0–40%) and increasing salt concentration (150–600 mM) on the interactions. All binding assays were exclusively performed in standard MST buffer (20 mM Tris-HCl pH 7.5, 150 mM NaCl, 10 mM MgCl<sub>2</sub>, 0.05% Tween, and 2 mM DTT). For dSpCas9–sgRNA interaction studies, experiments were carried out using a constant concentration of Cy5-sgRNA 500 (pM). Following this, a series of dilutions of dSpCas9 (ranging from 15 nM to 458 fM) was added into the sgRNA and incubated for 10–15 min at room temperature. In the case of binding studies for RNP and dsDNA, a complex of dSpCas9GFP–sgRNA (in a 1:2 ratio) was prepared, maintaining a protein concentration of 100 nM, and was incubated for 1 h at 21 °C. Following this, a series of dilutions of dsDNA (ranging from 10  $\mu$ M to 0.3 nM) was added into the RNP complex and incubated for 10–15 min at RT. The samples were then loaded onto capillaries. All measurements were carried out using a nanobluo detector at an excitation wavelength of 460–490 nM. All the data were collected in triplicate. The binding curves were fitted using MO. Affinity Analysis software (Nanotemper Technologies) and the processed data were plotted in OriginPro 8.5.

**Circular Dichroism Spectroscopy.** CD spectra were recorded for SpCas9 (2  $\mu$ M) protein in the presence of osmolytes (sucrose and glycerol) ranging 0–40% and increasing salt concentrations (150–600 mM). The spectra were recorded using a Jasco J-815 spectrometer with a cuvette of 0.1 cm path length, at a wavelength ranging between 190 and 250 nm. All samples were prepared in ITC buffer, and spectra were collected with an average of over 10 scans, at a scanning speed of 100 nm/min, and a temperature of 20 °C.

## RESULTS

**SpCas9 and SpCas9–sgRNA Show Enhanced Stability in the Presence of Osmolytes.** Our primary aim is to gain a thermodynamic understanding of the various interactions involved in the gene editing process facilitated by the SpCas9 protein. To achieve this, it is imperative to investigate these systems across different conditions and temperatures. Our initial focus is on examining how these conditions influence the stability of the Cas9 protein, enabling us to determine the optimal experimental conditions. Thus, we conducted experiments to determine the thermal unfolding profiles of SpCas9 protein in two distinct states: apo (lacking sgRNA) and RNP (with its cognate partner sgRNA). NanoDSF and UV melting were employed to probe the unfolding behavior across a temperature spectrum ranging between 20 and 80 °C with a rate change at 1 °C/s. As shown in (Figure 1 and Figure S1), the SpCas9 in the free form starts melting in the mid 30 °C range and has a melting temperature,  $T_m = 42.5$  °C (315.6 K). The RNP complex is more stable with a  $T_m = 49.2$  °C (322.3 K), and the onset for the thermal denaturation is closer to 40 °C. The  $T_{\text{onset}}$  temperatures were the upper limit at which the ITC and MST data were gathered. The melting results indicate that RNP complexes are more thermostable than free SpCas9 (Table S1).

Subsequently, we wanted to investigate the effect of osmolytes on the stability of protein and RNP complex. Initially, we assessed the thermal stability of the unbound protein in the presence of varying concentrations of glycerol and sucrose, spanning the range of 0–40% (Figure 2 and Figure S2). The increase in glycerol concentrations has been observed to enhance the stability of the protein, as evidenced by a notable increase in melting temperature  $T_m$  within the

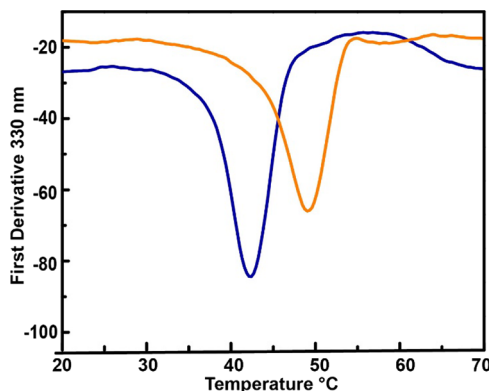


**Figure 1.** Thermal stability of SpCas9 and SpCas9-sgRNA by nanoDSF. The first derivative of the F 330 nm signal highlights the change in fluorescence intensity signifying the unfolding of protein and RNP. The inflection temperature of SpCas9 (blue) and SpCas9-sgRNA (orange) unfolding ( $T_m$ ) is determined as the peak of the curve.

range of 42–48 °C (Figure 2a). Similarly, an increase in glycerol concentrations also positively influenced the RNP complex stability  $T_m$  of 49–52 °C (Figure 2c). The results for sucrose also demonstrated enhanced stability (Figure 2b,d), as obtained for glycerol suggesting a common physiological effect of increasing osmolyte concentration on the stability of the SpCas9 and RNP complex.

Next, we expanded our studies to examine how different concentrations of neutral salt (NaCl), specifically, 150, 300, 450, and 600 mM, influence the stability of the SpCas9 protein. The increasing amount of salt enhanced the protein stability, as observed by enhanced  $T_m$  of 43.7–46.5 °C (Figure 3, Figure S3, and Table S1). The presence of salt appears to be positively correlated with the stability of the SpCas9 protein. This may be due to the principle similar to applied in the

“salting-in” effect, where salt ions stabilize the protein’s folded state. This occurs because the favorable interactions between the charged residues of the protein and their image charges lead to the enhancement of the protein folding state.<sup>16</sup> However, the enhancement in stability was not significantly observed in the RNP complex with increasing salt concentration (Figure 3b). The findings indicate that electrostatic forces play a significant role in forming interactions between SpCas9 and sgRNA. Nevertheless, the increase in salt concentration contributes modestly to maintaining the specific interactions between Cas9 and sgRNA once they are established.

**dSpCas9–sgRNA and RNP–dsVEGFA3 DNA Complex Exhibits Strong Binding Affinity.** The effectiveness and precision of CRISPR technology depend, in part, on the strength of the binding interactions between sgRNA and Cas9, as well as between the RNP complex and its corresponding target. Therefore, it is crucial that we measure the binding affinities of these interactions as accurately as possible. We utilized a comprehensive strategy, combining two complementary techniques: isothermal titration calorimetry (ITC) and microscale thermophoresis (MST), to precisely determine the binding affinity ( $K_a$ ). First, we used ITC wherein sgRNA was titrated into its cognate partner dSpCas9 protein at 298.15 K. A representative isotherm for the dSpCas9–sgRNA complex formation at 298.15 K is shown in Figure 4a. The dSpCas9 protein is a strong sgRNA binder with an estimated  $K_a = 2.3 \pm 0.3 \times 10^7 \text{ M}^{-1}$ . The ITC results were further verified by microscale thermophoresis (MST) for dSpCas9–sgRNA. At 298.15 K, a much higher binding association between dSpCas9 and sgRNA with a  $K_a = 8.61 \pm 0.91 \times 10^9 \text{ M}^{-1}$  was observed by MST (Figure 4c), which is ~100-fold higher compared to the binding affinity observed by the isothermal calorimetry. Differences in binding affinities observed between two orthologous techniques, ITC, and

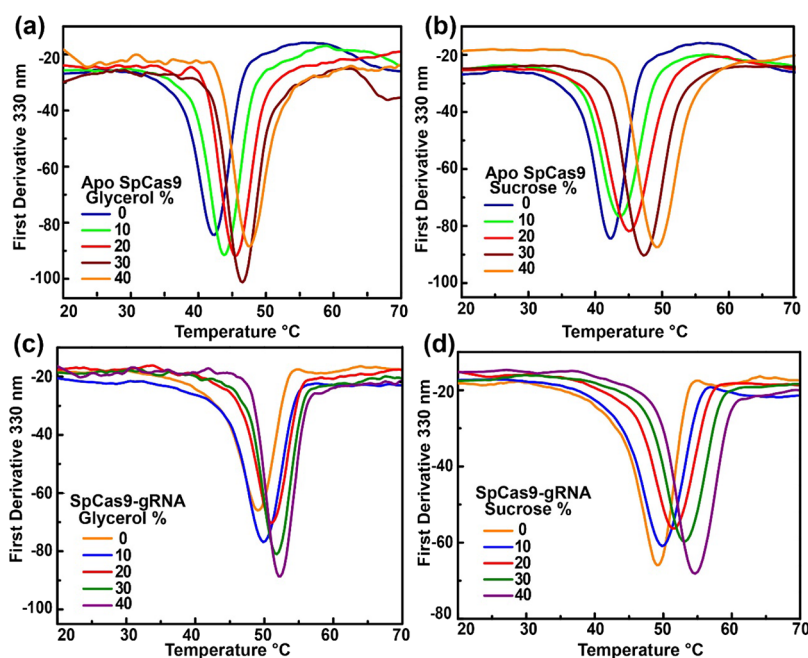


**Figure 2.** Thermal stability of SpCas9 and SpCas9-sgRNA in the presence of increasing concentration of glycerol and sucrose by nanoDSF. The first derivative of the fluorescence at 330 nm signal with an increasing percentage of glycerol and sucrose (0–40%) shows a shift in the  $T_m$  to higher temperatures indicating the enhancement in the stability of (a, b) free protein and (c, d) RNP complex.

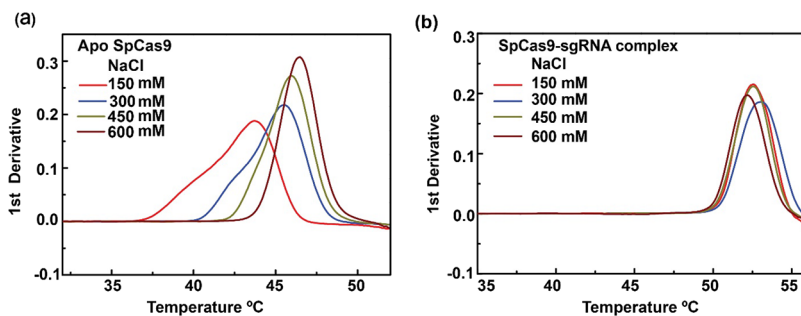


**Figure 3.** Thermal stability for free SpCas9 protein and SpCas9-sgRNA in the presence of an increasing concentration of NaCl using UV melting. (a) The first derivative at 280 nm for free protein indicated a shift in the  $T_m$  toward higher temperatures with increasing amounts of NaCl (150, 300, 450, and 600 mM). (b) No significant change in the  $T_m$  was observed in the RNP complex as the salt concentration increased.

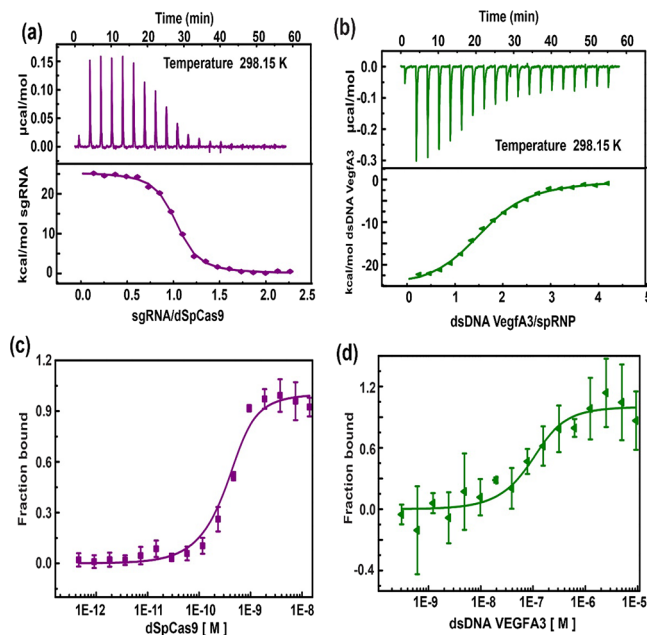


**Figure 4.** Representative isothermal titration calorimetry (ITC) isotherms and MST dose-response curve of interactions between dSpCas9-sgRNA and RNP-dsVEGFA3 DNA at 298.15 K. (a, b) The upper panels show raw ITC data for the endothermic interaction between dSpCas9-sgRNA and the exothermic interaction between RNP-dsDNAs. The lower panels display the integrated fitted heat plots for the interactions between dSpCas9-sgRNA and RNP-dsDNA at 298.15 K. (c, d) MST dose-response curve of the dSpCas9-sgRNA and RNP-dsDNA interactions at 298.15 K. Error bars depict standard deviation calculated from three identical replicates.

MST outcomes can hinge on two critical considerations: equilibration time<sup>17</sup> and buffer condition. Considering the former factor, it becomes evident that ITC captures the initial binding event, providing insights into the transient effect occurring immediately after mixing RNA and protein. In contrast, techniques like MST measure steady-state signals after longer equilibration. Additionally, variations in buffer conditions between ITC and MST can impact binding interactions. Thus, MST that measures the binding after a certain equilibration time provided us with a more accurate binding constant between SpCas9 and sgRNA as discussed below. This implies a greater uncertainty in the  $K_b$  values measured by ITC experiments, potentially compromising the accuracy of thermodynamic parameters such as Gibbs free energy ( $-\Delta G_{obs}$ ) calculations. As a result, for Gibbs free

energy calculations, we will use the  $K_b$  values obtained from MST studies.

To explore the association between the RNP (dSpCas9-sgRNA) and dsVEGFA3 DNA, we carried out interaction studies using both ITC and MST techniques. The dsVEGFA3 DNA was titrated on the dSpCas9gfp-sgRNA complex (3:1), exhibiting a binding association  $K_a = 1.4 \pm 0.08 \times 10^6 \text{ M}^{-1}$  (Figure 4b). Similarly, the dsVEGFA3 DNA in a series of dilutions was incubated with the dSpCas9gfp-sgRNA complex (1:2), and the measurement showed a binding association  $K_a = 1.95 \pm 0.15 \times 10^7 \text{ M}^{-1}$  (Figure 4d). The binding association of dsVEGFA3 DNA to dSpCas9gfp-sgRNA from MST is 10-fold higher compared to that observed by ITC. MST data is consistent with our previous findings.<sup>15</sup> This difference in binding affinities between the two orthologous techniques for the RNP-dsDNA complex is due to variations in binding buffer conditions as discussed below.

**dSpCas9 and Cognate sgRNA Is Entropically Driven, while dSpCas9-sgRNA (RNP)-dsVEGFA3 DNA Recognition Is Enthalpically Driven.** To determine the thermodynamic signatures characteristic of dSpCas9 and cognate sgRNA and dSpCas9-sgRNA (RNP)-dsVEGFA3 DNA bindings, we performed titrations by ITC. As described earlier, the measured association constants by MST experiments at 298.15 K were used to determine the Gibbs free energies ( $\Delta G$ )<sup>2</sup> utilizing standard eq 1.

Representative ITC isotherms for the formation of the dSpCas9 and cognate sgRNA and dSpCas9-sgRNA (RNP)-dsVEGFA3 DNA bindings are shown in Figure 4a,b. The enthalpy ( $\Delta H_{obs}$ ) measured via ITC experiments at 298.15 K was utilized to deduce the entropy changes using the standard eq 2.

All the obtained thermodynamic parameters are shown in Table 2. Both the binding isotherms were monophasic and exhibited molar equivalence points in the range of 1.0–1.6. The results indicate distinct thermodynamic profiles for the interactions between sgRNA and dSpCas9, as well as RNP and target dsDNA. For the dSpCas9-sgRNA interaction, a highly favorable Gibbs free energy change ( $\Delta G$ ) of  $-13.55 \pm 0.06 \text{ kcal}\cdot\text{mol}^{-1}$  suggests strong spontaneous binding but interestingly shows a positive enthalpy change ( $\Delta H_{obs}$ ) of  $24.7 \pm 0.9 \text{ kcal}\cdot\text{mol}^{-1}$  indicating an endothermic process. Additionally, the positive entropy change ( $\Delta S$ ) of  $128.2 \pm 3.0 \text{ cal}\cdot\text{mol}^{-1}\cdot\text{K}^{-1}$  suggests an increase in disorderliness upon binding. The positive entropy suggests a contribution from structural rearrangement, as observed in structural studies. Specifically, the Rec lobe adopts a more open conformation due to a significant rotation of the Rec-III domain, accompanied by

**Table 2.** Thermodynamic Parameters Were Measured for SpCas9-sgRNA and RNP–dsVEGFA3 DNA Complex Formations at 298.15 K<sup>a</sup>

	$K_a$ ( $M^{-1}$ ) <sup>b</sup>	$\Delta G_{obs}$	$\Delta G^2$	$\Delta H_{obs}^c$	$\Delta S$
		kcal·mol <sup>-1</sup>	kcal·mol <sup>-1</sup>	kcal·mol <sup>-1</sup>	cal·mol <sup>-1</sup> ·K <sup>-1</sup>
ITC	ITC				
dSpCas9–sgRNA	$2.30 \pm 0.30 \times 10^7$			$-10.04 \pm 0.09$	$24.70 \pm 0.90$
RNP–dsDNA	$1.40 \pm 0.08 \times 10^6$	$8.61 \pm 0.91 \times 10^9$		$-8.40 \pm 0.03$	$-24.06 \pm 3.20$
MST				$-9.94 \pm 0.05$	$-47.38 \pm 10.80$

<sup>a</sup>The thermodynamic parameters obtained from ITC measurements at 298.15 K are reported.<sup>2</sup>  $\Delta G$  was calculated at 298.15 K using equation  $\Delta G = -RT \ln K_a$

<sup>b</sup>The  $K_a$  is the binding constant measured from MST. Subsequently, the  $\Delta S$  was calculated using equation

$$\Delta G = \Delta H - T\Delta S \quad (2)$$

<sup>c</sup>The  $\Delta H_{obs}$  is the enthalpy change as measured by ITC.

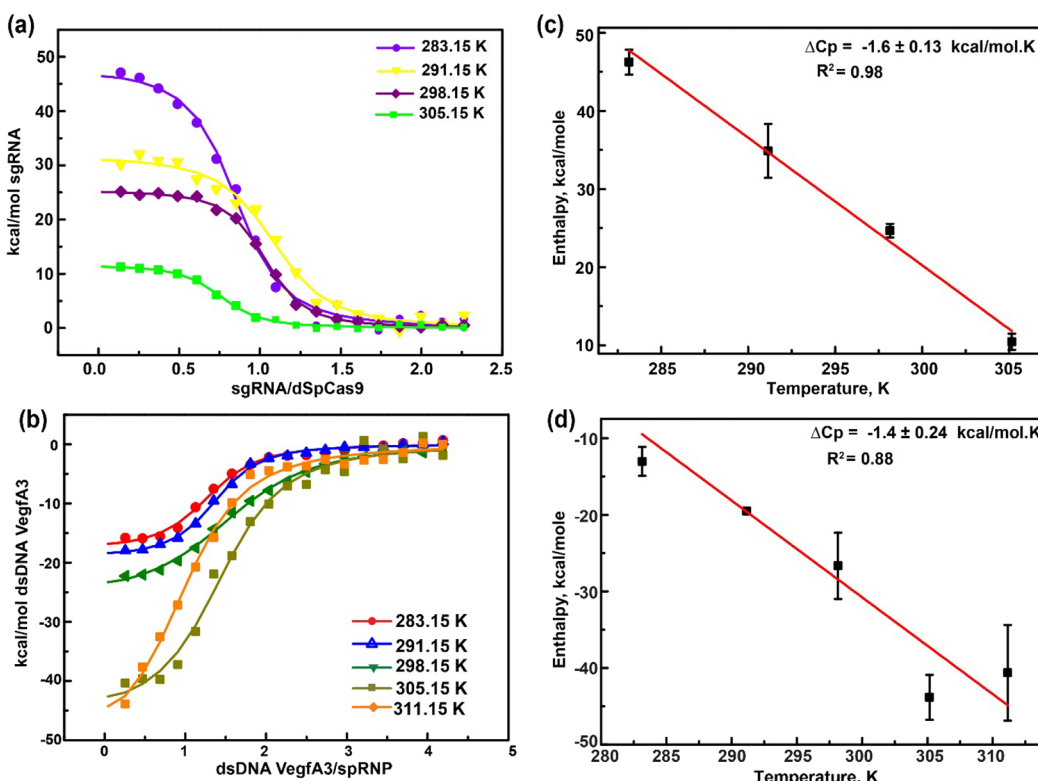


**Figure 5.** Representative fitted curve of isothermal titration calorimetry (ITC) of interaction between dSpCas9–sgRNA and dSpCas9–sgRNA with dsVEGFA3 DNA at different temperatures. (a, b) The superimposition of the fitted curve at various temperatures reveals a discernible decline in enthalpy for dSpCas9–sgRNA and an increase in enthalpy for dSpCas9–sgRNA–dsDNA with increasing temperature. (c, d) Correlation graph of enthalpy vs temperature for dSpCas9–sgRNA complex and RNP–dsDNA complex, the slope of which gives heat capacity and a coefficient of determination value.

smaller movements in other Rec domains to accommodate the sgRNA.<sup>18,19</sup> Conversely, the RNP–dsDNA interaction exhibits a slightly less favorable ( $\Delta G$ ) of  $-9.94 \pm 0.05$  kcal·mol<sup>-1</sup>, indicating spontaneous binding but to a lesser extent than the former interaction. The negative enthalpy change ( $\Delta H_{obs}$ ) of  $-24.06 \pm 3.2$  kcal·mol<sup>-1</sup> suggests an exothermic process, while the negative entropy change ( $\Delta S$ ) of  $-47.38 \pm 10.8$  cal·mol<sup>-1</sup>·K<sup>-1</sup> indicates a decrease in disorderliness upon binding. The negative entropy change reflects structural constraints, supporting the previous studies that show that the presence

of Mg<sup>2+</sup> helps the transition of HNH domain to adopt a compact and restrained catalytic conformation required for DNA cleavage.<sup>8,20,21</sup> In addition to conformational changes in Cas9, the uptake/release of ordered water molecules and counterions may contribute to entropy changes. Thus, to gain additional insights into the changes in the hydration state of dSpCas9 protein before and after the complex formation process, we measured changes in heat capacity ( $\Delta C_p$ ) on sgRNA and Cas9 complex formation.

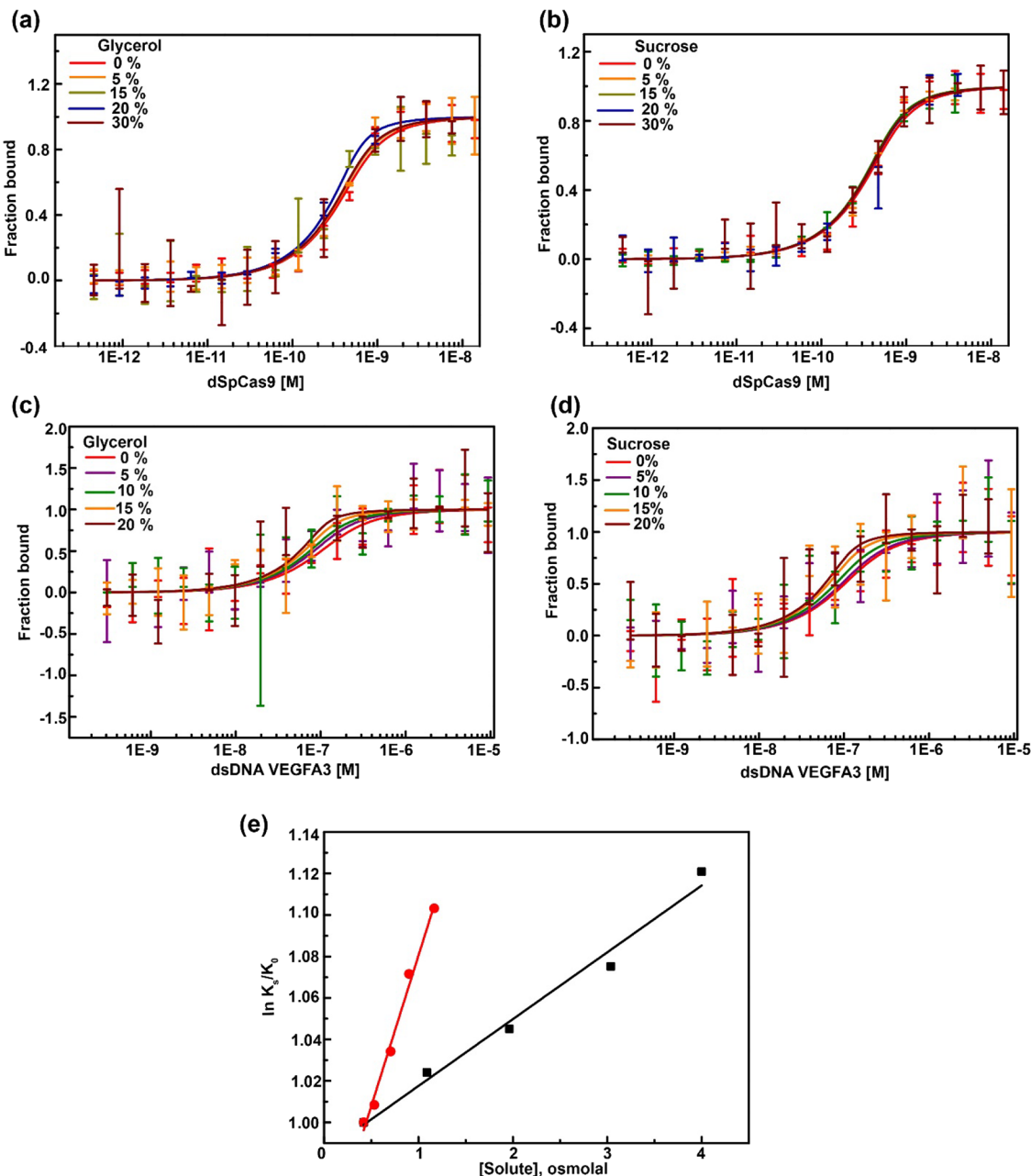


**Figure 6.** Osmolyte-induced effect on the binding constant of dSpCas9–sgRNA and RNP–dsDNA complex. (a, b) MST dose–response curves for dSpCas9–sgRNA (0–30%) and (c, d) RNP–dsVEGFA3 DNA complexes at increasing glycerol and sucrose concentrations (0–20%) at 298.15 K. (e) The natural logarithmic plot of association constant ( $K_a$ ) at various osmolyte concentrations relative to the binding constant at no osmolyte addition ( $K_0$ ) versus the osmolality at physiological salt (150 mM NaCl) at 298.15 K. The difference in water, however, depends on the solute;  $n_w = 2$  waters per complex for glycerol (black) and 8 for sucrose (red). This difference in water activity is the characteristic feature of reactions that involve the burial of exposed surface area.

**Formation of SpCas9-sgRNA and RNP–dsDNA Complexes Exhibit Negative Heat Capacity.** Heat capacity changes in biomolecular binding processes are crucial indicators of the underlying thermodynamic mechanisms driving molecular interactions. Understanding these changes provides insights into the energetics and structural dynamics involved, aiding in optimizing biomolecular assays and biotechnological applications.<sup>22–24</sup> In our next set of experiments, we determined the heat capacity changes ( $\Delta C_p$ ) for dSpCas9–sgRNA binding, which was calculated from the slope of the binding enthalpies ( $\Delta H_{obs}$ ) versus temperature plot at a range of temperatures (283.15–303.15 K) (Figure 5, Figure S4, and Table S2). The  $\Delta C_p$  value obtained for sgRNA–Cas9 complex formation is  $-1.6 \pm 0.13$  kcal/mol·K (Figure 5c). Similar studies for RNP–dsDNA binding resulted in a negative  $\Delta C_p$  of  $-1.4 \pm 0.24$  kcal/mol·K (Figure 5d, Figure S5, and Table S3). The negative  $\Delta C_p$  for the RNP–dsDNA complex is strongly suggestive of a phenomenon that involves the liberation of water or counterions from the binding interface of RNP to accommodate dsDNA. To better understand the changes in hydration and ionization state on complex formation, we further examined the effect of varying osmolytes and salt concentrations.

S4, and Table S2). The  $\Delta C_p$  value obtained for sgRNA–Cas9 complex formation is  $-1.6 \pm 0.13$  kcal/mol·K (Figure 5c). Similar studies for RNP–dsDNA binding resulted in a negative  $\Delta C_p$  of  $-1.4 \pm 0.24$  kcal/mol·K (Figure 5d, Figure S5, and Table S3). The negative  $\Delta C_p$  for the RNP–dsDNA complex is strongly suggestive of a phenomenon that involves the liberation of water or counterions from the binding interface of RNP to accommodate dsDNA. To better understand the changes in hydration and ionization state on complex formation, we further examined the effect of varying osmolytes and salt concentrations.

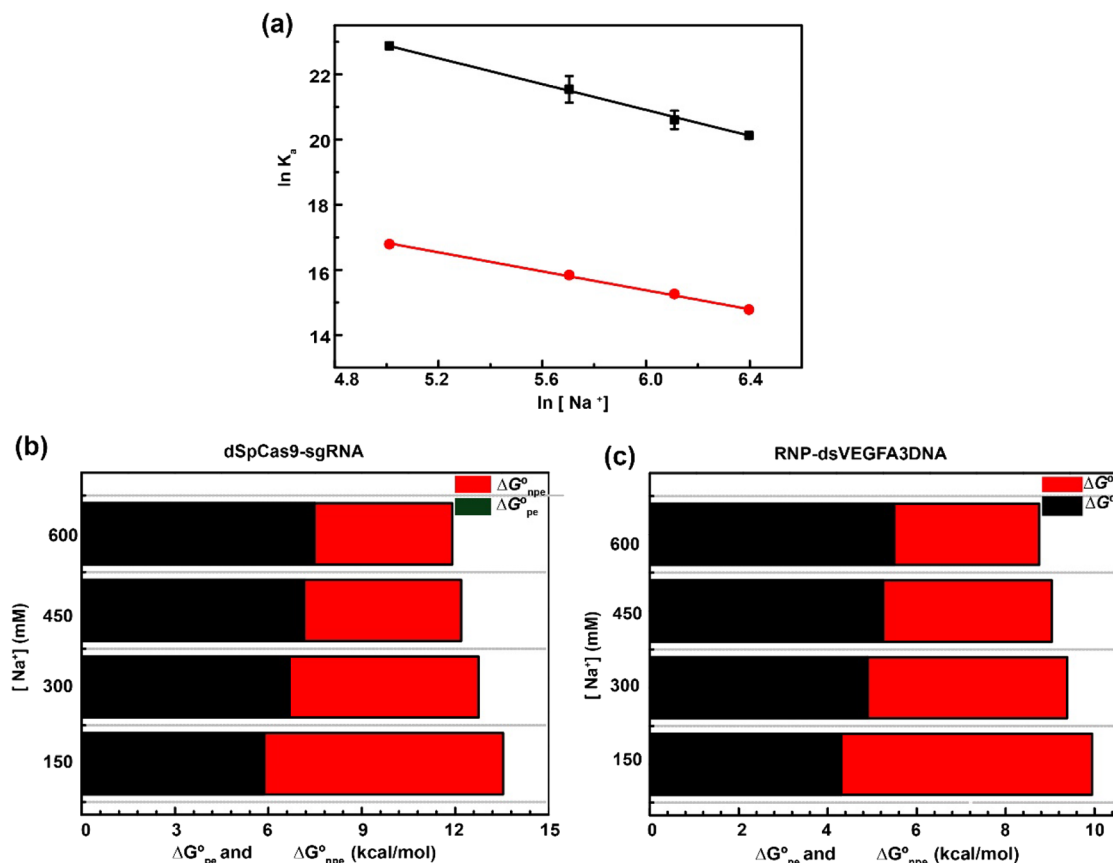


**Figure 7.** Polyelectrolyte effects dominate the free energy of SpCas9-sgRNA and RNP-dsDNA recognition. (a) The natural logarithmic variation of the association constant ( $K_a$ ) with respect to the concentration of  $Na^+$  ions ( $\log[Na^+]$ ) upon dSpCas9–sgRNA (black) and RNP–dsDNA (red) complex formation. (b, c) The dissection of the total free energy into polyelectrolytic contribution ( $G_{PE}$ ), as well as the nonpolyelectrolyte effect ( $G_{nPE}$ ) contribution, is represented in the graph.

**Uptake/Release of Water Molecules upon sgRNA–Cas9 and RNP–dsDNA Interactions.** The observed heat capacity changes in the Cas9–sgRNA and RNP complex–duplex DNA interaction suggest a significant role for water molecules in the binding process. Water mediates biomolecular interactions, facilitating the formation of hydrogen bonds crucial for stabilizing the complex. The rearrangement of water molecules in the hydration shell surrounding the complex likely contributes to the observed heat capacity changes. Studying water's involvement in the binding process is essential as it provides insights into the thermodynamics of complex formation. Therefore, investigating water's role merits attention for a comprehensive understanding of Cas9-mediated genome editing and potential therapeutic applications. The osmotic stress method has been widely employed to assess the involvement of water molecules in diverse biochemical reactions.<sup>25–27</sup> Any equilibrium involving alterations in water molecules associated with a biopolymer is sensitive to changes in water activity ( $aW$ ).<sup>31</sup> Water activity can be modulated by adding low molecular weight cosolutes, which, while not interacting with the biopolymer, are presumed to alter water activity. Equation 3 can be used to quantify the number of water molecules involved in the binding event:

$$\partial \ln(K_s/K_0)/\partial [Osm] = -n_w/55.5 \quad (3)$$

The change in binding energy, denoted as  $\ln(K_s/K_0)$ , is influenced by the osmolality (moles of solute/kg of solvent) of the solution, represented by “Osm”, and  $\Delta n_w$ , which signifies

the variance in the number of bound water molecules between the complex and the free reactants.<sup>28</sup> Thus, the binding constants were measured at increasing concentrations of these osmolytes (glycerol and sucrose 0–30%) for dSpCas9–sgRNA protein and (glycerol and sucrose 0–20%) for RNP–dsDNA. MST was used to measure the binding affinity with increasing concentrations of osmolyte (glycerol and sucrose) for both complexes (Figure 6 and Table S4). Figure 6a,b shows that the increase in osmolyte concentrations does not have much effect on the binding affinity of dSpCas9–sgRNA. However, there is an increase in the binding affinity of RNP with dsDNA (Figure 6c,d). This increase in  $K_a$  observed in the presence of osmolyte indicates the expulsion of the water molecules from the binding surface during interactions.<sup>29</sup> Figure 6c,d shows the change in binding affinity upon the change in osmolyte concentrations. The average water molecules released are 2 and  $8 \pm 1$  in glycerol and sucrose, respectively (Figure 6e). However, the release of tightly bound water molecules from the binding site can lead to an increase in heat capacity due to the disruption of water's hydrogen bonding network, but in contradiction, we observed a large negative heat capacity change. This contradicting observation indicates that there is a large structural rearrangement and energetic adjustments occurring upon dSpCas9–sgRNA and RNP–dsDNA complex formation.

**Polyelectrolyte Effects on the Binding Constants of dSpCas9–sgRNA and RNP–dsDNA Complexes.** The negative change in heat capacity ( $\Delta C_p$ ) also serves as an

indicator of ionization alterations in biomolecular interactions. Thus, we further delved into the impact of heightened ionic strength on the bonding between sgRNA and dSpCas9 and dsDNA with the RNP complex. Given the substantial role of electrostatic interactions in governing DNA/RNA binding to proteins, examining the effects of elevated salt concentration offers valuable insights into the underlying mechanics of these interactions. Our investigations involved MST experiments conducted under varying salt conditions of 150, 300, 450, and 600 mM [Na<sup>+</sup>] (see Figure S6). The relationship between the binding constant and Na<sup>+</sup> concentration can be expressed as

$$\partial \ln(K_a) / \partial \ln[\text{Na}^+] = -n\Psi = (SK) \quad (4)$$

Here, [Na<sup>+</sup>] denotes the sodium ion concentration, *n* represents the number of ionic bonds formed between the phosphate oxygen atoms of the nucleic acids and the positively charged amino acids side chains of the protein, and  $\Psi$  defines the fraction of sodium ions bound to the phosphate group. An increase in ionic strength revealed a decrease in the association constant,  $K_a$ , of sgRNA and dSpCas9 as well as RNP–dsDNA (refer to Table 2). This decrease in the association constant is attributed to the sodium ions initially bound to the RNA or dsDNA phosphate groups, experiencing a reduced gain in entropy of mixing upon release into bulk solution in the presence of the high salt environment. The slope of  $\ln K_a$  plotted against  $\ln[\text{Na}^+]$ ,  $SK = n\Psi$ , quantifies the count of released ions condensed on the RNA/dsDNA backbone to the bulk solution during the formation of ionic bonds with the charged amino-acid side chains. The variation of  $\ln K_a$  plotted against  $\ln[\text{Na}^+]$  reveals a linear relationship, the slope ( $SK$ ) of which provides the value of  $-1.98 \pm 0.02$  for dSpCas9–sgRNA and  $-1.48 \pm 0.03$  for RNP–dsDNA (see Figure 7a). This indicates the release of only a few (less than two) counterions condensed on the backbone of either RNA and dsDNA upon binding. This observation contradicts the findings from crystal structures of the complexes, which clearly demonstrate numerous interactions between positively charged protein residues and both sgRNA and dsDNA within the complexes. However, similar observations have been noted in various protein–nucleic acid interactions. For instance, analysis of salt concentration-dependent  $K_a$  data for proteins such as HMG-box, TBP, and IHF revealed that the estimated number of released counterions is significantly lower than the number of protein–DNA ion pairs observed in crystal structures.<sup>30–32</sup>

Further, the observed Gibbs free energy was partitioned into contributions from polyelectrolytic ( $\Delta G^\circ_{\text{pe}}$ ) and nonpolyelectrolytic ( $\Delta G^\circ_{\text{npe}}$ ) in Table 3. The polyelectrolytic contribution or the free-energy contribution due to ion release can be obtained using the equation:

$$\Delta G^\circ_{\text{pe}} = (-SK)RT \ln[\text{Na}^+] \quad (5)$$

and

$$\Delta G^\circ_{\text{pe}} = (\Delta G^\circ_{\text{obs}} - \Delta G^\circ_{\text{npe}}) \quad (6)$$

Figure 7b,c shows the parsing of free energy for the interaction between sgRNA–dSpCas9 and dsDNA–RNP complex. At a [Na<sup>+</sup>] concentration of 150 mM, the contribution of  $\Delta G^\circ_{\text{pe}}$  for binding of sgRNA to dSpCas9 has been determined to be  $-5.87$  kcal/mol and for dsDNA–RNP  $-4.3$  kcal/mol. This is 43.35 and 43.25%, the percentage contribution of  $\Delta G^\circ_{\text{pe}}$  to total Gibbs free energy ( $\Delta G^\circ_{\text{obs}}$ ) for

**Table 3. MST Measured Binding Constants for dSpCas9–sgRNA and RNP–dsVEGFA3 DNA with Increasing Salt Concentration**

[Na <sup>+</sup> ] (mM)	$K^\alpha \times 10^9$ (M <sup>-1</sup> )	$\Delta G^\circ$ (kcal·mol <sup>-1</sup> )	$\Delta G^\circ_{\text{pe}}$ (kcal·mol <sup>-1</sup> )	$\Delta G^\circ_{\text{npe}}$ (kcal·mol <sup>-1</sup> )
dSpCas9–sgRNA				
150	$8.61 \pm 0.91$	-13.54	-5.87	-7.67
300	$2.38 \pm 0.85$	-12.75	-6.68	-6.07
450	$0.91 \pm 0.23$	-12.19	-7.16	-5.03
600	$0.54 \pm 0.01$	-11.91	-7.49	-4.42
RNP–dsDNA				
	$K^\alpha \times 10^7$ (M <sup>-1</sup> )			
150	$1.96 \pm 0.16$	-9.94	-4.30	-5.64
300	$0.76 \pm 0.07$	-9.38	-4.89	-4.48
450	$0.42 \pm 0.04$	-9.04	-5.25	-3.79
600	$0.26 \pm 0.01$	-8.76	-5.49	-3.26

<sup>a</sup> $\Delta G^\circ$  was calculated using the standard equation  $\Delta G = -RT \ln K_a$  for dSpCas9–sgRNA and RNP–dsDNA complexes. Following this, division of free energy between polyelectrolyte and nonpolyelectrolyte contribution is done using the equation  $\Delta G^\circ = \Delta G^\circ_{\text{pe}} + \Delta G^\circ_{\text{npe}}$ .

sgRNA–dSpCas9 and RNP–dsDNA complex, respectively. Furthermore, at physiological salt concentration, the data is suggestive of the favorable nonpolyelectrolytic component ( $\Delta G^\circ_{\text{npe}}$ )  $-7.67$  kcal/mol (dSpCas9–sgRNA) and  $-5.64$  kcal/mol (RNP–dsDNA) making substantial (~56% of total free energy) contribution in formation of complexes. Thus, the data at physiological salt concentration is in agreement that the association constants for both RNA–protein and RNP–dsDNA, which are primarily governed by nonpolyelectrolytic effects, encompassing conformational alterations upon complex formation, the intricate interplay of hydrophobic forces, hydrogen bonds, van der Waals, and dipole–dipole interactions.<sup>33,25</sup>

## ■ DISCUSSION

Thermodynamic studies play a pivotal role in advancing our understanding of the sgRNA–Cas9 interaction and the formation of ribonucleoprotein (RNP) complexes with cognate duplexes in the CRISPR–Cas9 genome editing system. These studies provide essential insights into the energetics and molecular mechanisms underlying CRISPR-mediated genome editing, facilitating the optimization of CRISPR-based technologies for various applications. Understanding the thermodynamic parameters, such as binding enthalpy, entropy change, and heat capacity change, offers valuable information regarding the specificity, efficiency, and stability of the sgRNA–Cas9 interaction and RNP complex formation. Moreover, thermodynamic analyses contribute to the rational design of CRISPR systems, guiding the selection of optimal sgRNA sequences and target sites to enhance editing precision and minimize off-target effects. By elucidating the thermodynamic principles governing CRISPR interactions, these studies drive innovation in gene-editing methodologies, opening avenues for therapeutic interventions, functional genomics, and agricultural biotechnology, thereby shaping the future of genetic engineering and precision medicine.

Our studies first reveal that SpCas9 and SpCas9–sgRNA in the presence of osmolytes are more thermostable. Nevertheless, studies show no significant effect of osmolytes on the native structure of the protein.<sup>34,35</sup> Similar outcomes were observed in our research, where increasing concentrations of glycerol and sucrose did not notably influence the secondary

structure of the SpCas9 protein as indicated by circular dichroism (CD) data (Figure S7). Interestingly, the increase in salt concentration ( $\text{NaCl}$ ) induces subtle changes in secondary structure, and the SpCas9 protein showed two negative peaks at 207 and 220 nm, which suggests the existence of  $\alpha$ -helix structure (Figure S8). The increase in ionic strength shows a decrease in negative peak at 207 nm suggesting conformational changes in protein. Additionally, the increasing salt concentration leads to SpCas9 protein stability, and this effect can be attributed to the increase in solvent surface tension at a higher salt concentration that can further enhance hydrophobic force and thus stabilize the protein core or native protein fold.<sup>36</sup>

Inspection of Table 2 reveals a notable discrepancy in the  $K_b$  values derived from MST and ITC data, differing by approximately 100-fold for sgRNA–Cas9 interaction and 10-fold for RNP complex-duplex DNA interactions at 25 °C. For accurate determination of the binding constant in a bimolecular interaction, it is important to consider the technique used, whether it reports steady-state binding affinity after long equilibration or captures transient effects. ITC falls into the latter category, which explains the greater variation in binding affinity observed between ITC and MST in the SpCas9-sgRNA system. This discrepancy is more pronounced because sgRNA is a slow-binding ligand. The SpCas9 interaction with sgRNA may be a two-step binding process with distinctly different kinetic association rates. In ITC the fast step will dominate the output providing us with a binding affinity of the first encounter between SpCas9 and sgRNA and thus missing out on the information about the second step restructuring of the complex toward a higher affinity complex. Thus, we are getting the apparent  $K_b$  with ITC that is larger than the actual  $K_b$ . On the other hand, MST, which is a steady-state technique will determine the actual  $K_b$  since the binding affinity, is measured after a long equilibration time.<sup>19</sup> Inspection of MST data further elucidates that the intermolecular interactions between SpCas9 protein and sgRNA result in a strong picomolar affinity for each other. A similar picomolar affinity between biomolecules is seen when an RNA substrate fits well into the specific moieties and/or binding pockets of the protein, leading to highly effective binding.<sup>37</sup> Additionally, the variation in buffer and the presence of Tween 0.05% may lead to a higher binding affinity; however, for dSpCas9–sgRNA, we did not see much of a difference (Figures S9a and Table S5). The difference in binding affinity for RNP-dsDNA between ITC and MST is due to the presence of the 0.05% Tween 20 in the buffer (Figure S9b and Table S5). The increase in binding affinity measured by ITC in the presence of the nonionic detergent suggests that conformational changes may occur, leading to higher binding affinity.

The thermodynamic parameters associated with the interaction between sgRNA and SpCas9 provide valuable insights into the nature of these molecular binding events. The negative value of the Gibbs free energy change ( $\Delta G = -13.55 \pm 0.06 \text{ kcal/mol}$ ) indicates that the formation of the sgRNA–spCas9 complex is energetically favorable, suggesting that the molecules tend to associate spontaneously under the given conditions. The positive enthalpy change ( $\Delta H = 24.70 \pm 0.90 \text{ kcal/mol}$ ) suggests that energy is absorbed from the surroundings during complex formation, indicating an endothermic process. Although the protein can engage in hydrogen bonding, van der Waals interactions, hydrophobic interactions,  $\pi$  interactions, and stacking interactions with RNA bases, the 2'-OH group, and the phosphodiester

backbone, all of these result in negative enthalpy change.<sup>37,38</sup> However, SpCas9- and sgRNA-binding results in a positive enthalpy change suggesting the contribution of two factors: the breaking of existing hydrogen bonds and the rearrangement of molecular structures to facilitate complex formation.<sup>6,39</sup> Additionally, the positive entropy change ( $\Delta S = 128.20 \pm 3.00 \text{ cal/mol-K}$ ) implies an increase in molecular disorder or randomness upon complex formation. This increase in entropy contributes favorably to the spontaneity of the interaction, offsetting the endothermic nature of the process. The positive entropy in protein–RNA interaction can be attributed to the local rearrangement of biomolecules that exhibit backbone shifts and residues and bases to flip out leading to binding dynamics during protein–RNA interactions.<sup>40–43</sup> The two biomolecules may become rigid at the sites of interactions but adjacent residues may become more flexible compensating for a decrease in entropy.<sup>43</sup> Additionally, the unstructured loops in RNA and disordered linkers in proteins are regions that undergo rearrangements in RNA–protein binding contributing to the positive entropy.<sup>44–46</sup> Jinek et al. in 2014 and Jiang et al. in 2015 resolved the apo and sgRNA-bound Cas9 structures from *Streptococcus pyogenes* (PDB 4CMQ and PDB 4ZT0) at resolutions of 3.09 and 2.9 Å, respectively.<sup>47,48</sup> Their findings unveiled a notable rearrangement in the helical REC domains of Cas9 upon sgRNA binding (Figure 8a,b).

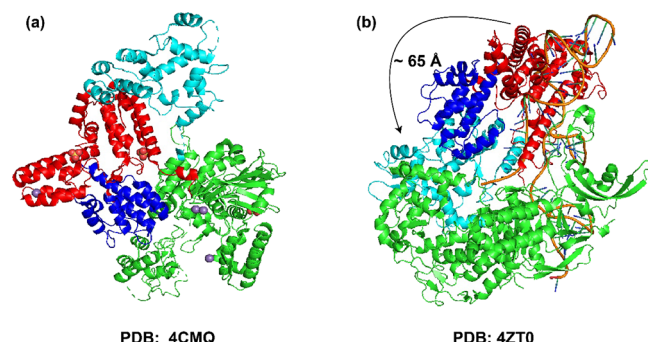


**Figure 8.** Crystal structure of apo SpCas9 and SpCas9-sgRNA. (a) Crystal structure showing apo form of SpCas9 protein. The domain in red is Rec-I, navy blue is Rec-II domain, cyan is Rec-III domain, and green is NUC domain. (b) The crystal structure showing the conformational rearrangement of Rec-III domain of SpCas9 protein upon sgRNA binding.

This rearrangement was marked by a significant  $\sim 65 \text{ \AA}$  shift of the REC-III domain to accommodate the sgRNA molecule. The positive entropy change observed in the interaction between sgRNA and Cas9, indicating increased disorder or randomness upon complex formation, can be correlated with the significant rearrangement of the REC domains of Cas9, particularly the  $\sim 65 \text{ \AA}$  shift of the REC-III domain to accommodate the sgRNA molecule. This rearrangement likely involves the disruption of existing molecular structures and the creation of new conformational states, leading to increased flexibility and disorder within the system. Additionally, the positive entropy change observed suggests the release of water molecules and counterions during complex formation.<sup>49</sup> Therefore, the  $\sim 65 \text{ \AA}$  shift of the REC-III domain in Cas9 to accommodate sgRNA likely results in increased molecular dynamics and conformational flexibility, along with the release of ions, contributing to the positive entropy change observed in the sgRNA–Cas9 complex formation. This correlation

highlights the intimate relationship between structural rearrangements and thermodynamic changes in molecular interactions, underscoring the importance of considering both aspects in understanding the underlying mechanisms of complex formation.

Next, our investigation discloses the binding energetics between RNP and dsDNA. The negative value of the Gibbs free-energy change ( $\Delta G = -9.94 \pm 0.05$  kcal/mol) indicates that the interaction between RNP and dsDNA is thermodynamically favorable, suggesting that the formation of the complex is spontaneous under the given conditions. The negative enthalpy change ( $\Delta H = -24.06 \pm 3.20$  kcal/mol) suggests that the interaction between RNP and dsDNA is exothermic, meaning it releases heat to the surroundings during complex formation. This negative enthalpy change may arise from the formation of new bonds or interactions (specific or nonspecific) between the molecules, which release energy. Structural studies have shown that in the RNP complex, in addition to specific interactions, Cas9 engages in numerous nonspecific interactions with the phosphate backbone of ntDNA. These nonspecific interactions between Cas9 (HNH, RuvC, and PI domains) and ntDNA are essential for the stability of the R-loop structure.<sup>50</sup> Apart from sgRNA:tDNA base pairing, the RNP-dsDNA is further stabilized by nonspecific interactions between the negatively charged backbone of tDNA with the positively charged Cas9 residues (R66, R70, and R74 of the bridge-helix). It is worth noting that the negative enthalpy change is opposed by unfavorable entropy change typically seen for most biomolecular interactions.<sup>33</sup> The RNP-dsDNA complex results in a negative entropy change ( $\Delta S = -47.38 \pm 10.80$  cal/mol·K), indicating a decrease in disorder or randomness upon complex formation. This negative entropy change may be attributed to the restriction of molecular motions or conformational changes that occur when RNP and dsDNA bind to each other. The cryo-electron microscopy (cryo-EM) structures of Cas9:sgRNA:dsDNA in the presence of Mg<sup>2+</sup> unveiled three distinct states (precatalytic, PDB: 6O0Z; postcatalytic, 6O0Y; product, 6O0X), emphasizing the critical role of Mg<sup>2+</sup> in stabilizing the catalytic residues of Cas9 around the scissile phosphate and facilitating target DNA (tDNA) cleavage.<sup>51</sup> In the context of Cas9–sgRNA-duplex binding, the rotation of the HNH domain, driven by Mg<sup>2+</sup> binding, brings the catalytic H840 residue closer to the cleavage site on the target DNA strand. This conformational change is essential for the activation of Cas9's endonuclease activity, allowing it to precisely cleave the target DNA.<sup>11,52,53</sup> The negative entropy change observed in this process is likely associated with the conformational rearrangements and structural constraints imposed on the complex upon Mg<sup>2+</sup> binding and HNH domain rotation.<sup>20</sup> As the HNH domain rotates to position the catalytic residue for cleavage, it may restrict the flexibility and freedom of movement within the complex, leading to a decrease in molecular disorder or entropy.

In our temperature-dependent isothermal titration calorimetry (ITC) study, we observed that the binding of sgRNA to SpCas9 is accompanied by a negative heat capacity change ( $-1.6 \pm 0.13$  kcal/mol·K). This negative heat capacity change ( $\Delta C_p$ ) alongside a positive entropy change ( $\Delta S$ ) in spCas9–sgRNA interactions can be attributed to various molecular processes. Our subsequent investigation using osmotic stress revealed minimal involvement of water molecules in the interaction. Therefore, a plausible explanation is that the

binding of RNA and protein induces conformational changes in both molecules. These changes, such as the burial of hydrophobic surfaces or the formation of hydrogen bonds, restrict the conformational flexibility of the molecules, leading to a negative heat capacity change ( $\Delta C_p < 0$ ). The interplay between the displacement of water molecules and conformational dynamics highlights the intricate thermodynamic behavior governing molecular recognition processes in SpCas9–sgRNA protein interactions.

Our studies further demonstrate that electrostatic interactions dominate the binding between SpCas9–sgRNA and RNP-dsDNA. We looked into the crystal structure of this complex solved by Nureki and colleagues (PDB: 4O08). Although SpCas9–sgRNA–dsDNA is a large complex and thus makes several interactions between positively charged protein residues and sgRNA and dsDNA. Interestingly, the crystal structure of the complex unveils that conserved arginine cluster on the bridge helix, which represents a universal structural characteristic found in all Cas9 proteins.<sup>6</sup> This cluster of six arginines plays a crucial role by forming essential interactions with both RNA and DNA. Particularly, R66, R70, and R74 are majorly involved, as these form multiple salt bridges with stem-loop 1 of sgRNA and with DNA in the RNP-dsDNA complex<sup>6</sup> (Figure S10). Our studies unveil the release of two counterions condensed on RNA backbone on SpCas9–sgRNA complex formation, and similar results were seen for dsDNA on RNP-dsDNA binding, suggesting that arginines may be involved in the electrostatic interactions with the sgRNA and DNA, respectively.<sup>11</sup>

Our studies provide crucial insights into how this work can enhance CRISPR–Cas9 technology. We observed that increasing the concentration of osmolytes, such as glycerol and sucrose, improved the thermal stability of both apo Cas9 and SpCas9–sgRNA. Extensive research has explored the effects of osmolytes on protein folding, structure, and function.<sup>54–56</sup> While the binding affinity between dSpCas9–sgRNA remained largely unaffected by increased osmolyte concentration, the RNP-dsDNA complex exhibited higher affinity under these conditions. Thus, we assume that the presence of osmolyte can readily improve the cleavage efficiency of the CRISPR–Cas9 system. Our studies also provide insights into the optimal temperature for efficient interactions between Cas9–sgRNA and the RNP–dsVEGFA3 DNA complex. Specifically, for the RNP–dsVEGFA3 DNA complex, we observed an increase in enthalpy as the temperature rose, with a significant increase from  $-24$  to  $-44.5$  kcal/mol as the temperature ranged from 298.15 to 305.15 K. This huge enthalpy jump suggests the structural alterations in the RNP complex upon binding to dsVEGFA3 DNA. Notably, the enthalpy values at different temperatures do not exhibit a linear correlation, as indicated by an  $R^2$  value of 0.88 (Figure Sd). This deviation suggests that the RNP–dsVEGFA3 DNA-binding interactions are coupled with conformational changes, as supported by structural studies.<sup>18,57</sup> Our findings indicate that domain rearrangement within the SpCas9 protein in the RNP complex occurs upon dsVEGFA3 DNA binding at higher temperatures, a critical transformation necessary for its proper cleavage activity. Thus, our research supports that the efficient cleavage temperature is above 33 °C. This is well supported by previous studies where dsVEGFA3 target dsDNA is efficiently cleaved at 33 °C or higher by CRISPR–Cas9.<sup>58</sup>

In summary, our investigations have uncovered crucial understandings regarding the thermodynamic landscape of

interactions between CRISPR Cas9–sgRNA and CRISPR RNP-target DNA. It is worth noting that these interactions are influenced by physiological factors such as temperature, osmolytes, and ionic strength. This underscores the significance of considering the effects of environmental conditions on CRISPR–Cas9 interactions, revealing the intricate dynamics among molecular components across varied settings.

## ■ ASSOCIATED CONTENT

### Data Availability Statement

All the data is available within the manuscript and supplementary figures/tables.

### ■ Supporting Information

The Supporting Information is available free of charge at <https://pubs.acs.org/doi/10.1021/acs.jpcb.4c04044>.

Supplementary figures and tables ([PDF](#))

### Accession Codes

Q99ZW2 · CAS9\_STRP1

## ■ AUTHOR INFORMATION

### Corresponding Authors

**Niyati Jain** — CSIR-Institute of Genomics & Integrative Biology, New Delhi 110025, India; Academy of Scientific and Innovative Research (AcSIR), Ghaziabad 201002, India;  
 [orcid.org/0000-0002-1524-2411](https://orcid.org/0000-0002-1524-2411); Email: [niyati2002us@gmail.com](mailto:niyati2002us@gmail.com)

**Souvik Maiti** — CSIR-Institute of Genomics & Integrative Biology, New Delhi 110025, India; Academy of Scientific and Innovative Research (AcSIR), Ghaziabad 201002, India;  
 [orcid.org/0000-0001-9897-1419](https://orcid.org/0000-0001-9897-1419); Email: [souvik@igib.res.in](mailto:souvik@igib.res.in)

### Authors

**Ajit Kumar** — CSIR-Institute of Genomics & Integrative Biology, New Delhi 110025, India; Academy of Scientific and Innovative Research (AcSIR), Ghaziabad 201002, India

**Purba Daripa** — CSIR-Institute of Genomics & Integrative Biology, New Delhi 110025, India

**Kaiser Rasool** — CSIR-Institute of Genomics & Integrative Biology, New Delhi 110025, India

**Debojyoti Chakraborty** — CSIR-Institute of Genomics & Integrative Biology, New Delhi 110025, India; Academy of Scientific and Innovative Research (AcSIR), Ghaziabad 201002, India;  [orcid.org/0000-0003-1460-7594](https://orcid.org/0000-0003-1460-7594)

Complete contact information is available at:  
<https://pubs.acs.org/10.1021/acs.jpcb.4c04044>

### Author Contributions

S.M. was responsible for conceptualization. A.K., P.D., and K.R. were responsible for methodology and investigation. S.M. and N.J. were responsible for data curation. A.K., S.M., and N.J. were responsible for validation. S.M., N.J., and D.C. were responsible for resources. S.M. and N.J. were responsible for writing. S.M. and N.J. were responsible for supervision. S.M. and N.J. were responsible for funding acquisition. All authors approve the submission of this manuscript.

### Notes

The authors declare no competing financial interest.

## ■ ACKNOWLEDGMENTS

S.M. and N.J. acknowledge the support of the MLP2009 project from the Council of Scientific and Industrial Research (CSIR, India). N.J. is supported by the Department of Biotechnology, Government of India-Ramalingaswami fellowship grant (BT/RLF/Re-entry/HRD/35/2019), Department of Biotechnology (DBT). A.K. is supported by a Senior Research Fellowship (SRF) from the Department of Biotechnology (DBT), India. The authors acknowledge Dr. Saji Menon Application Scientist Nanotemper Technologies Bengaluru, India for helping to collect the data on Monolith NT.115 Pico.

## ■ REFERENCES

- (1) Frangoul, H.; Altshuler, D.; Cappellini, M. D.; Chen, Y.-S.; Domm, J.; Eustace, B. K.; Foell, J.; De la Fuente, J.; Grupp, S.; Handgretinger, R.; et al. CRISPR-Cas9 Gene Editing for Sickle Cell Disease and  $\beta$ -Thalassemia. *N. Engl. J. Med.* **2021**, *384* (3), 252–260.
- (2) Garneau, J. E.; Dupuis, M.-È.; Villion, M.; Romero, D. A.; Barrangou, R.; Boyaval, P.; Fremaux, C.; Horvath, P.; Magadán, A. H.; Moineau, S. The CRISPR/Cas Bacterial Immune System Cleaves Bacteriophage and Plasmid DNA. *Nature* **2010**, *468* (7320), 67–71.
- (3) Deltcheva, E.; Chylinski, K.; Sharma, C. M.; Gonzales, K.; Chao, Y.; Pirzada, Z. A.; Eckert, M. R.; Vogel, J.; Charpentier, E. CRISPR RNA Maturation by Trans-Encoded Small RNA and Host Factor RNase III. *Nature* **2011**, *471* (7340), 602–607.
- (4) Jinek, M.; Chylinski, K.; Fonfara, I.; Hauer, M.; Doudna, J. A.; Charpentier, E. A Programmable Dual-RNA-Guided DNA Endonuclease in Adaptive Bacterial Immunity. *Science* **2012**, *337* (6096), 816–821.
- (5) Cong, L.; Ran, F. A.; Cox, D.; Lin, S.; Barretto, R.; Habib, N.; Hsu, P. D.; Wu, X.; Jiang, W.; Marraffini, L. A.; Zhang, F. Multiplex Genome Engineering Using CRISPR/Cas Systems. *Science* **2013**, *339* (6121), 819 LP–823.
- (6) Nishimasu, H.; Ran, F. A.; Hsu, P. D.; Konermann, S.; Shehata, S. I.; Dohmae, N.; Ishitani, R.; Zhang, F.; Nureki, O. Crystal Structure of Cas9 in Complex with Guide RNA and Target DNA. *Cell* **2014**, *156* (5), 935–949.
- (7) East, K. W.; Newton, J. C.; Morzan, U. N.; Narkhede, Y. B.; Acharya, A.; Skeens, E.; Jogl, G.; Batista, V. S.; Palermo, G.; Lisi, G. P. Allosteric Motions of the CRISPR-Cas9 HNH Nuclease Probed by NMR and Molecular Dynamics. *J. Am. Chem. Soc.* **2020**, *142* (3), 1348–1358.
- (8) Dagdas, Y. S.; Chen, J. S.; Sternberg, S. H.; Doudna, J. A.; Yildiz, A. A Conformational Checkpoint between DNA Binding and Cleavage by CRISPR-Cas9. *Sci. Adv.* **2017**, *3* (8), No. eaao0027.
- (9) Singh, D.; Sternberg, S. H.; Fei, J.; Doudna, J. A.; Ha, T. Real-Time Observation of DNA Recognition and Rejection by the RNA-Guided Endonuclease Cas9. *Nat. Commun.* **2016**, *7* (1), 12778.
- (10) Singh, D.; Wang, Y.; Mallon, J.; Yang, O.; Fei, J.; Poddar, A.; Ceylan, D.; Bailey, S.; Ha, T. Mechanisms of Improved Specificity of Engineered Cas9s Revealed by Single-Molecule FRET Analysis. *Nat. Struct. Mol. Biol.* **2018**, *25* (4), 347–354.
- (11) Maghsoud, Y.; Jayasinghe-Arachchige, V. M.; Kumari, P.; Cisneros, G. A.; Liu, J. Leveraging QM/MM and Molecular Dynamics Simulations to Decipher the Reaction Mechanism of the Cas9 HNH Domain to Investigate Off-Target Effects. *J. Chem. Inf. Model.* **2023**, *63* (21), 6834–6850.
- (12) Saha, A.; Pindi, C.; Palermo, G. The Synchronized Catalytic Dance of CRISPR-Cas9. *Nat. Catal.* **2023**, *6* (10), 870–872.
- (13) Raper, A. T.; Stephenson, A. A.; Suo, Z. Functional Insights Revealed by the Kinetic Mechanism of CRISPR/Cas9. *J. Am. Chem. Soc.* **2018**, *140* (8), 2971–2984.
- (14) Kumar, A.; Daripa, P.; Maiti, S.; Jain, N. Interaction of HnRNPB1 with Helix-12 of HHOTAIR Reveals the Distinctive Mode of RNA Recognition That Enables the Structural Rearrangement by LCD. *Biochemistry* **2023**, *62* (13), 2041–2054.

- (15) Acharya, S.; Mishra, A.; Paul, D.; Ansari, A. H.; Azhar, M.; Kumar, M.; Rauthan, R.; Sharma, N.; Aich, M.; Sinha, D.; Sharma, S. Francisella Novicida Cas9 Interrogates Genomic DNA with Very High Specificity and Can Be Used for Mammalian Genome Editing. *Proc. Natl. Acad. Sci. U. S. A.* **2019**, *116* (42), 20959–20968.
- (16) Beauchamp, D. L.; Khajehpour, M. Studying Salt Effects on Protein Stability Using Ribonuclease T1 as a Model System. *Biophys. Chem.* **2012**, *161*, 29–38.
- (17) Jarmoskaite, I.; AlSadhan, I.; Vaidyanathan, P. P.; Herschlag, D. How to Measure and Evaluate Binding Affinities. *Elife* **2020**, *9*, No. e57264.
- (18) Sternberg, S. H.; LaFrance, B.; Kaplan, M.; Doudna, J. A. Conformational Control of DNA Target Cleavage by CRISPR-Cas9. *Nature* **2015**, *527* (7576), 110–113.
- (19) Palermo, G.; Miao, Y.; Walker, R. C.; Jinek, M.; McCammon, J. A. CRISPR-Cas9 Conformational Activation as Elucidated from Enhanced Molecular Simulations. *Proc. Natl. Acad. Sci. U. S. A.* **2017**, *114* (28), 7260–7265.
- (20) Nierwizki, L.; East, K. W.; Binz, J. M.; Hsu, R. V.; Ahsan, M.; Arantes, P. R.; Skeens, E.; Pacesa, M.; Jinek, M.; Lisi, G. P.; Palermo, G. Principles of Target DNA Cleavage and the Role of Mg<sup>2+</sup> in the Catalysis of CRISPR-Cas9. *Nat. Catal.* **2022**, *5* (10), 912–922.
- (21) Wang, Y.; Mallon, J.; Wang, H.; Singh, D.; Hyun Jo, M.; Hua, B.; Bailey, S.; Ha, T. Real-Time Observation of Cas9 Postcatalytic Domain Motions. *Proc. Natl. Acad. Sci. U. S. A.* **2021**, *118* (2), No. e2010650118.
- (22) Prabhu, N. V.; Sharp, K. A. Heat Capacity in Proteins. *Annu. Rev. Phys. Chem.* **2005**, *56*, 521–548.
- (23) Takach, J. C.; Mikulecky, P. J.; Feig, A. L. Salt-Dependent Heat Capacity Changes for RNA Duplex Formation. *J. Am. Chem. Soc.* **2004**, *126* (21), 6530–6531.
- (24) Mikulecky, P. J.; Feig, A. L. Heat Capacity Changes Associated with DNA Duplex Formation: Salt- and Sequence-Dependent Effects. *Biochemistry* **2006**, *45* (2), 604–616.
- (25) Suryawanshi, H.; Sabharwal, H.; Maiti, S. Thermodynamics of Peptide-RNA Recognition: The Binding of a Tat Peptide to TAR RNA. *J. Phys. Chem. B* **2010**, *114* (34), 11155–11163.
- (26) Parsegian, V. A.; Rand, R. P.; Rau, D. C. Macromolecules and Water: Probing with Osmotic Stress. *Methods Enzymol.* **1995**, *259*, 43–94.
- (27) Robinson, C. R.; Sligar, S. G. Hydrostatic and Osmotic Pressure as Tools to Study Macromolecular Recognition. *Methods Enzymol.* **1995**, *259*, 395–427.
- (28) Qu, X.; Chaires, J. B. Hydration Changes for DNA Intercalation Reactions. *J. Am. Chem. Soc.* **2001**, *123* (1), 1–7.
- (29) Record, M. T. Jr.; Ha, J. H.; Fisher, M. A. Analysis of Equilibrium and Kinetic Measurements to Determine Thermodynamic Origins of Stability and Specificity and Mechanism of Formation of Site-Specific Complexes between Proteins and Helical DNA. *Methods Enzymol.* **1991**, *208*, 291–343.
- (30) O'Brien, R.; DeDecker, B.; Fleming, K. G.; Sigler, P. B.; Ladbury, J. E. The Effects of Salt on the TATA Binding Protein-DNA Interaction from a Hyperthermophilic Archaeon. *J. Mol. Biol.* **1998**, *279* (1), 117–125.
- (31) Holbrook, J. A.; Tsodikov, O. V.; Saecker, R. M.; Record, M. T. Jr. Specific and Non-Specific Interactions of Integration Host Factor with DNA: Thermodynamic Evidence for Disruption of Multiple IHF Surface Salt-Bridges Coupled to DNA Binding. *J. Mol. Biol.* **2001**, *310* (2), 379–401.
- (32) Dragan, A. I.; Read, C. M.; Makeyeva, E. N.; Milgotina, E. I.; Churchill, M. E. A.; Crane-Robinson, C.; Privalov, P. L. DNA Binding and Bending by HMG Boxes: Energetic Determinants of Specificity. *J. Mol. Biol.* **2004**, *343* (2), 371–393.
- (33) Samatanga, B.; Cléry, A.; Barraud, P.; Allain, F. H.-T.; Jelesarov, I. Comparative Analyses of the Thermodynamic RNA Binding Signatures of Different Types of RNA Recognition Motifs. *Nucleic Acids Res.* **2017**, *45* (10), 6037–6050.
- (34) Melo, E. P.; Estrela, N.; Lopes, C.; Matias, A. C.; Tavares, E.; Ochoa-Mendes, V. Compacting Proteins: Pros and Cons of Osmolyte-Induced Folding. *Curr. Protein Pept. Sci.* **2010**, *11* (8), 744–751.
- (35) Manning, M. C.; Chou, D. K.; Murphy, B. M.; Payne, R. W.; Katayama, D. S. Stability of Protein Pharmaceuticals: An Update. *Pharm. Res.* **2010**, *27* (4), 544–575.
- (36) Jiang, L.; Wang, Z.; Li, Y.; Meng, X.; Sui, X.; Qi, B.; Zhou, L. Relationship Between Surface Hydrophobicity and Structure of Soy Protein Isolate Subjected to Different Ionic Strength. *Int. J. Food Prop.* **2015**, *18* (5), 1059–1074.
- (37) Corley, M.; Burns, M. C.; Yeo, G. W. How RNA-Binding Proteins Interact with RNA: Molecules and Mechanisms. *Mol. Cell* **2020**, *78* (1), 9–29.
- (38) Teplova, M.; Malinina, L.; Darnell, J. C.; Song, J.; Lu, M.; Abagyan, R.; Musunuru, K.; Teplov, A.; Burley, S. K.; Darnell, R. B.; Patel, D. J. Protein-RNA and Protein-Protein Recognition by Dual KH1/2 Domains of the Neuronal Splicing Factor Nova-1. *Structure* **2011**, *19* (7), 930–944.
- (39) Chen, L.; Brügger, K.; Skovgaard, M.; Redder, P.; She, Q.; Torarinsson, E.; Greve, B.; Awayez, M.; Zibat, A.; Klenk, H. P.; Garrett, R. A. The Genome of Sulfolobus Acidocaldarius, a Model Organism of the Crenarchaeota. *J. Bacteriol.* **2005**, *187* (14), 4992–4999.
- (40) Yang, Y.; Declerck, N.; Manival, X.; Aymerich, S.; Kochoyan, M. Solution Structure of the LicT-RNA Antitermination Complex: CAT Clamping RAT. *EMBO J.* **2002**, *21* (8), 1987–1997.
- (41) Hainzl, T.; Huang, S.; Sauer-Eriksson, A. E. Structural Insights into SRP RNA: An Induced Fit Mechanism for SRP Assembly. *RNA* **2005**, *11* (7), 1043–1050.
- (42) Matthews, M. M.; Thomas, J. M.; Zheng, Y.; Tran, K.; Phelps, K. J.; Scott, A. I.; Havel, J.; Fisher, A. J.; Beal, P. A. Structures of Human ADAR2 Bound to dsRNA Reveal Base-Flipping Mechanism and Basis for Site Selectivity. *Nat. Struct. Mol. Biol.* **2016**, *23* (5), 426–433.
- (43) Leulliot, N.; Varani, G. Current Topics in RNA-Protein Recognition: Control of Specificity and Biological Function through Induced Fit and Conformational Capture. *Biochemistry* **2001**, *40* (27), 7947–7956.
- (44) Treger, M.; Westhof, E. Statistical Analysis of Atomic Contacts at RNA-Protein Interfaces. *J. Mol. Recognit.* **2001**, *14* (4), 199–214.
- (45) Han, K.; Nepal, C. PRI-Modeler: Extracting RNA Structural Elements from PDB Files of Protein-RNA Complexes. *FEBS Lett.* **2007**, *581* (9), 1881–1890.
- (46) Barik, A.; C, N.; Pilla, S. P.; Bahadur, R. P. Molecular Architecture of Protein-RNA Recognition Sites. *J. Biomol. Struct. Dyn.* **2015**, *33* (12), 2738–2751.
- (47) Jinek, M.; Jiang, F.; Taylor, D. W.; Sternberg, S. H.; Kaya, E.; Ma, E.; Anders, C.; Hauer, M.; Zhou, K.; Lin, S.; Kaplan, M.; Iavarone, A. T.; Charpentier, E.; Nogales, E.; Doudna, J. A. Structures of Cas9 Endonucleases Reveal RNA-Mediated Conformational Activation. *Science* **2014**, *343* (6176), No. 1247997.
- (48) Jiang, F.; Zhou, K.; Ma, L.; Gressel, S.; Doudna, J. A. STRUCTURAL BIOLOGY. A Cas9-Guide RNA Complex Preorganized for Target DNA Recognition. *Science* **2015**, *348* (6242), 1477–1481.
- (49) Sakamoto, T.; Ennifar, E.; Nakamura, Y. Thermodynamic Study of Aptamers Binding to Their Target Proteins. *Biochimie* **2018**, *145*, 91–97.
- (50) Ray, A.; Di Felice, R. Protein-Mutation-Induced Conformational Changes of the DNA and Nuclease Domain in CRISPR/Cas9 Systems by Molecular Dynamics Simulations. *J. Phys. Chem. B* **2020**, *124* (11), 2168–2179.
- (51) Zhu, X.; Clarke, R.; Puppala, A. K.; Chittori, S.; Merk, A.; Merrill, B. J.; Simonović, M.; Subramanian, S. Cryo-EM Structures Reveal Coordinated Domain Motions That Govern DNA Cleavage by Cas9. *Nat. Struct. Mol. Biol.* **2019**, *26* (8), 679–685.
- (52) Zhao, L. N.; Mondal, D.; Warshel, A. Exploring Alternative Catalytic Mechanisms of the Cas9 HNH Domain. *Proteins* **2020**, *88* (2), 260–264.

- (53) Yoon, H.; Zhao, L. N.; Warshel, A. Exploring the Catalytic Mechanism of Cas9 Using Information Inferred from Endonuclease VII. *ACS Catal.* **2019**, *9* (2), 1329–1336.
- (54) Mojtabavi, S.; Samadi, N.; Faramarzi, M. A. Osmolyte-Induced Folding and Stability of Proteins: Concepts and Characterization. *Iran. J. Pharm. Res. IJPR* **2019**, *18* (Suppl1), 13–30.
- (55) Auton, M.; Rösger, J.; Sinev, M.; Holthauzen, L. M. F.; Bolen, D. W. Osmolyte Effects on Protein Stability and Solubility: A Balancing Act between Backbone and Side-Chains. *Biophys. Chem.* **2011**, *159* (1), 90–99.
- (56) Rabbani, G.; Choi, I. Roles of Osmolytes in Protein Folding and Aggregation in Cells and Their Biotechnological Applications. *Int. J. Biol. Macromol.* **2018**, *109*, 483–491.
- (57) Jiang, F.; Taylor, D. W.; Chen, J. S.; Kornfeld, J. E.; Zhou, K.; Thompson, A. J.; Nogales, E.; Doudna, J. A. Structures of a CRISPR-Cas9 R-Loop Complex Primed for DNA Cleavage. *Science* **2016**, *351* (6275), 867–871.
- (58) Xiang, G.; Zhang, X.; An, C.; Cheng, C.; Wang, H. Temperature Effect on CRISPR-Cas9Mediated Genome Editing. *J. Genet. Genomics* **2017**, *44* (4), 199–205.